Author Manuscript

Author Manuscript

Author Manuscript

Author Manuscript

HHS Public Access

Author manuscript

Mol Cancer Ther. Author manuscript; available in PMC 2019 December 01.

Published in final edited form as:

Mol Cancer Ther. 2018 December ; 17(12): 2575–2585. doi:10.1158/1535-7163.MCT-18-0186.

Dual targeting of aurora kinases with AMG 900 exhibits potent preclinical activity against acute myeloid leukemia with distinct post-mitotic outcomes

Marc Payton[1,^], **Hung-Kam Cheung**[2], **Maria Stefania S. Ninniri**[1], **Christian Marinaccio**[3], **William C. Wayne**[1], **Kelly Hanestad**[1], **John D. Crispino**[3], **Gloria Juan**[2], and **Angela Coxon**[1]

[1]Amgen Discovery Research, Thousand Oaks, California

[2]Amgen Medical Sciences, Thousand Oaks, California

[3]Division of Hematology/Oncology, Northwestern University, Chicago, Illinois.

Abstract

Aurora kinase A and B have essential and non-overlapping roles in mitosis, with elevated expression in a subset of human cancers, including acute myeloid leukemia (AML). In this study, pan-aurora kinase inhibitor (AKI) AMG 900 distinguishes itself as an anti-leukemic agent that is more uniformly potent against a panel of AML cell lines than are isoform-selective AKIs and classic AML drugs. AMG 900 inhibited AML cell growth by inducing polyploidization and/or apoptosis. AMG 900 and aurora-B selective inhibitor AZD1152-hQPA showed comparable cellular effects on AML lines that do not harbor a *FLT3*-ITD mutation. AMG 900 was active against P-glycoprotein-expressing AML cells resistant to AZD1152-hQPA and was effective at inducing expression of megakaryocyte-lineage markers (CD41, CD42) on human CHRF-288–11 cells and mouse *Jak2*^{V617F} cells. In MOLM-13 cells, inhibition of p-histone H3 by AMG 900 was associated with polyploidy, extra centrosomes, accumulation of p53 protein, apoptosis, and cleavage of Bcl-2 protein. Co-administration of cytarabine (Ara-C) with AMG 900 potentiated cell killing in a subset of AML lines, with evidence of attenuated polyploidization. AMG 900 inhibited the proliferation of primary human bone marrow cells in culture, with a better proliferation recovery profile relative to classic anti-mitotic drug docetaxel. *In vivo*, AMG 900 significantly reduced tumor burden in a systemic MOLM-13 xenograft model where we demonstrate the utility of 3'-deoxy-3'–^{18}F-fluorothymidine [^{18}F]FLT positron emission tomographic (PET)–computed tomographic (CT) imaging to measure the anti-proliferative effects of AMG 900 in skeletal tissues in mice.

Keywords

AMG 900; AML; aurora kinase; mitosis

[^]Corresponding Author: Marc N. Payton, Discovery Research, Amgen Inc., One Amgen Center Thousand Oaks CA 91320. Phone: (805) 447-6697; mpayton@amgen.com.

Disclosure of Potential Conflicts of Interest. M. Payton, K. Cheung, W. Wayne, K. Hanestad, G. Juan, and A. Coxon are current or former full-time employees of Amgen Inc. and have owned stock in Amgen Inc. at the time this work was conducted. No potential conflicts of interest were disclosed by the other authors.

Author Manuscript Author Manuscript Author Manuscript Author Manuscript

Introduction

AML is a genetically heterogeneous disease that accounts for approximately 33% of newly diagnosed adult leukemia (1). In AML, defects in myeloid-lineage differentiation leads to clonal expansion of precursor cells that is fueled by pro-proliferative and pro-survival pathway signaling. Standard-of-care therapy for most younger adult AML patients is high-dose induction chemotherapy (daunorubicin and Ara-C) followed by post-remission treatments that include additional chemotherapy (consolidation) as well as allogeneic stem cell transplantation (2). Recently, the first multi-targeted kinase inhibitor (midostaurin) was approved in combination with chemotherapy for treating newly diagnosed AML patients with *FLT3* mutations (3). Elderly AML patients are often unfit for the intensive chemotherapy and therefore rely on less effective therapies such as low-dose Ara-C (LDAC). Furthermore, the disease in elderly AML patients may have unfavorable characteristics (*TP53* mutations, chromosome 5q and 7q deletions, P-glycoprotein (P-gp) expression) that have limited benefit from current therapies (4).

Aurora kinases (AK) A and B are essential mitotic regulators having both distinct functions and subcellular localization (5). The expression of aurora-A and -B is elevated in a variety of human cancers, including AML (6–8). The spindle assembly checkpoint (SAC) is a surveillance mechanism that governs mitotic progression by ensuring proper microtubule-attachment to sister chromatids at the kinetochore to achieve bipolar orientation and tension at metaphase. A classic hallmark of mitosis is the phosphorylation of histone H3 on serine-10 (p-histone H3) by aurora-B. Selective aurora-A inhibition leads to an increase in p-histone H3 and SAC activation which delays mitotic progression, whereas selective aurora-B or dual AK inhibition leads to a decrease in p-histone H3 and SAC silencing resulting in exit from mitosis without division (5).

MLN8054 and MLN8237 (alisertib) are isoform-selective inhibitors of aurora-A (9, 10), whereas AZD1152-hQPA (barasertib) targets aurora-B and FLT3 kinase activity with a 1000-fold selectivity over aurora-A (11, 12). In clinical studies, alisertib and barasertib have shown single-agent anti-leukemia activity in AML [overall response rate of 17% (pretreated, NCT00830518) and 35% (older newly diagnosis, NCT00952588), respectively] with on-target toxicities observed in proliferating normal tissues (13–15). Recent studies have shown that MLN8237 induces differentiation of acute megakaryoblastic leukemia (AMKL) cells, with potent anti-leukemia activity (16–18); these findings have led to a clinical study specifically targeting AMKL and primary myelofibrosis (PMF) (NCT02530619). Factors limiting the efficacy of AKIs may include quiescence (arrested state), such as in leukemic stem cells (19, 20); expression of drug-efflux transporters such as P-gp and BCRP1 (21, 22); and acquisition of target-modifying mutations in *AURKA* or *AURKB* (23, 24). To our knowledge, an inhibitor that is equipotent against aurora-A and -B and highly selective against other kinases has not been evaluated against isoform-selective AKIs in a panel of AML cell lines.

AMG 900 is a potent and highly selective pan-AKI with activity across solid tumor cell lines *in vitro,* and is effective at inhibiting the growth of taxane-resistant tumor xenografts *in vivo* (24–26). A recent study demonstrated that AMG 900 is more lethal to breast cancer cells

Author Manuscript Author Manuscript Author Manuscript Author Manuscript

with p53 pathway dysfunction (27). In combination studies, AMG 900 can potentiate the activity of histone deacetylase inhibitors and microtubule-targeting agents in preclinical tumor models (26, 28). In a phase-1 dose escalation study in AML patients (relapsed/refractory, NCT01380756), AMG 900 had a response rate of 9% (3-of-35 achieved a complete response with an incomplete count recovery), with cases of prolonged cytopenia, a prototypical AKI class effect (29).

In this report, we describe the effects of AMG 900, isoform-selective AKIs, and two classic anti-AML drugs on a diverse panel of AML cell lines. We assess the activity of AMG 900 on P-gp expressing AML cells, and its effects on expression of megakaryocyte-lineage markers as well as p53 and intrinsic apoptosis signaling pathways. We combine LDAC with AMG 900 in a subset of AML lines and perform expanded single-agent drug action studies using MOLM-13 cells and human bone marrow mononuclear cells (HBMNC) in culture. We investigate the anti-leukemia effects of AMG 900 using a systemic MOLM-13 xenograft model and evaluate the anti-proliferative response using PET/CT imaging to measure the level of [^{18}F]FLT in skeletal tissue in mice.

Materials and Methods

Small molecules.

AKIs include AMG 900 (in-house synthesis), MLN8054/MLN8237 (Selleck Chemicals), and AZD1152-hQPA (in-house synthesis); molecular structures have previously been reported (25). Test compounds include Ara-C (Sigma), daunorubicin (Sigma), docetaxel (Sanofi-Aventis), nocodazole (Sigma), nutlin-3a (Sigma), and GF120918 (Sigma) (30).

Cells and culture conditions.

Human AML cell lines were procured from ATCC or DSMZ and authenticated by ATCC using short tandem repeat DNA analysis. MOLM-13-Luc cell line expressing luciferase was established at Amgen Inc. (31). MOLM-13-Luc cells were negative for mycoplasma by DNA analysis (Charles River), the remaining AML cell lines have not been recently retested for the presence of mycoplasma. Cell lines were grown using recommended culture conditions and maintained at 37°C with 5% CO_2, a subset of lines were grown in the presence of penicillin/streptomycin (Invitrogen). Primary human bone marrow mononuclear cells (LONZA) were grown in 15% FBS in IMDM media supplemented with 2.5 ng/mL G-CSF, 2.5 ng/mL GM-CSF, and 10 ng/mL SCF (R&D Systems). To differentiate primary mouse bone marrow cell cultures to megakaryocytic lineage, c-kit+ progenitor cells were positively enriched from whole bone marrow obtained from *Jak2*^{V617F} knock-in mice using MACS system (Miltenyi Biotech). Enriched c-kit+ progenitor cells were grown in StemSpan Media (Stemcell Technologies) supplemented with 10 ng/mL mouse IL-3, 10 ng/mL human IL-6, 40 ng/mL mouse SCF, and 20 μg/mL human low-density lipoprotein (Stemcell Technologies) for 24 hours. Megakaryocytic differentiation was performed by culturing cells in 10% FBS in RPMI1640 media supplemented with 50 ng/mL mouse thrombopoietin (Stemcell Technologies).

Author Manuscript Author Manuscript Author Manuscript Author Manuscript

Animals.

All experimental procedures were conducted in accordance with the Institutional Animal Care and Use Committee Protocol at Molecular Imaging Inc. (Ann Arbor, Michigan), the U.S. Department of Agriculture regulations, and met all the Association for Assessment and Accreditation of Laboratory Animal Care specifications. NOD/SCID IL-2Rγ−/− (NSG) mice (Jackson Laboratory) were housed in sterilized cages maintained under aseptic and pathogen-free conditions. Food, water, and nutritional supplements were offered on a daily basis during the study. AMG 900 was formulated as a suspension in 2% HPMC, 1% Tween-80, at pH 2.2 and administered based on individual body weight.

Western blot analysis.

Whole cell lysates were prepared using RIPA Buffer (Sigma) supplemented with protease and phosphatase inhibitor cocktail (Roche). Primary antibodies [cl-caspase-3 (04–439), Bcl-2 (05–729), Bax (MAB4601) Millipore; p53 (9282), Mcl-1 (5453), GAPDH (14C10) CST; p21 (sc-6246) SCBT; MDM2 (MA1–113) Invitrogen; Bcl-xL (ab98143) Abcam; aurora-A (610938), aurora-B (611082) BD Biosciences; β-actin (A5441) Sigma]. Secondary detection performed using anti-rabbit or anti-mouse IgG Vectastain ABC kit (Vector Laboratories) and detected with Lightning-ECL kit (PerkinElmer).

Confocal imaging.

MOLM-13 cells were treated with AMG 900 at 10 nmol/L or DMSO for 48 hours. Formaldehyde (4%) fixed cells were stained with anti-p-histone H3 (05–806, Millipore) and anti-pericentrin antibodies (ab4448, Abcam). Secondary detection was performed using anti-mouse-alexa555 (A21422) and anti-rabbit-alexa488 (A11008) antibodies from Invitrogen and DNA was stained with 4’,6-diamidino-2-phenylindole (DAPI, CalBiochem). Stained cells were spotted on glass slides, treated with antifade reagent (Invitrogen), and mounted with coverslips in preparation for confocal imaging using Nikon Eclipse TE2000 inverted microscope (60x objective) running Nikon Elements software.

In vivo imaging.

NSG female mice were injected intravenous (IV) with 5×10^4 human MOLM-13-Luc luciferase cells. Xenogen IVIS bioluminescence (BLI) imaging platform (PerkinElmer) was used to acquire whole body BLI for each animal to confirm tumor establishment. Mice were injected intraperitoneal (IP) with 150 mg/kg of luciferin based on body weight and imaged 10 to15 minutes later as per manufactures instructions. Whole body [^{18}F]FLT-PET/CT imaging was conducted using sequential Siemens Focus micro-PET (200uCi [^{18}F]FLT IV, 60 minute incubation time, followed by 10 minute static scan) and Gamma Medica FLEX micro-CT (80 kVp, 440 uA). Nine days after tumor injection, mice with tumor burden were randomized into three treatment groups (n = 10 per group): vehicle alone (7 days daily, oral (PO)), AMG 900 at 22 mg/kg (4 days daily, PO), and AMG 900 at 12.6 mg/kg (7 days daily, PO). [^{18}F]FLT measurements were recorded at baseline (one day before treatment) and on days 5, 8, 11, and 14 post-treatment start. BLI measurements were collected on day 1 (before dosing on the day of treatment initiation) and on days 6, 9, 12, 15 post-treatment start. Data is represented as mean whole body BLI signal (photons/second, as per Xenogen

Author Manuscript Author Manuscript Author Manuscript Author Manuscript

instructions) or mean skeleton [^{18}F]FLT signal ± SEM. To quantify skeleton [^{18}F]FLT signal, a custom analysis program created by inviCRO Inc. (Boston, MA) was used to capture the whole body skeletal bone volume based on CT segmentation algorithm. CT derived skeleton regions-of-interest were used to quantitate the percentage of injected [^{18}F]FLT dose per gram of tissue (%ID/g). Statistical significance for [^{18}F]FLT and BLI was determined by comparing treated groups versus vehicle-control group using paired t-test. Study and image analysis was performed by inviCRO Inc..

Details about high-content cell imaging and flow cytometry (FC) assays are described in the Supplementary Materials and Methods.

Results

AMG 900 blocks proliferation of AML cell lines through polyploidization and apoptosis, with a distinct sensitivity profile relative to isoform-selective AKIs.

We first investigated the anti-proliferative effects of three AKIs [AMG 900 (pan), AZD1152-hQPA (B-selective), and MLN8054 (A-selective)] as well as Ara-C and daunorubicin in a panel of AML cell lines. Cells were treated with each test agent for 72 hours and processed for FC to measure absolute cell count, cell death (apoptosis and subG_1), and polyploidy (≥ 4N DNA content) (Supplementary Fig. S1A and B). As shown in Figure 1A, AMG 900 inhibited the growth of AML lines at low nanomolar concentrations, with largely uniform potency relative to the other test agents. The level of polyploidization and cell death induced by AMG 900 varied across AML lines, with three principal phenotypes observed polyploidy or cell death alone, and most frequently polyploidy with cell death (Fig. 1B and Supplementary Fig. S1C and D). The FLT3-ITD-expressing MOLM-13 and MV-411 cells showed a bell-shaped polyploidy profile with AZD1152-hQPA, in contrast to a stable polyploidy profile with AMG 900, consistent with a recent study identifying FLT3-ITD in AML as a target of AZD1152-hQPA (12). The cell-cycle effects observed with Ara-C (S-phase) and daunorubicin (G_2M) were distinct from AKI mode-of-action (Supplementary Fig. S1E).

Next, we determined the AKI effective concentration for either SAC activation or silencing by monitoring p-histone H3 levels. As shown in Figure 1C, inhibition of aurora-B activity by AMG 900 or AZD1152-hQPA led to p-histone H3 decrease and SAC silencing. In agreement with cell count data (in Fig. 1A), the two erythroleukemic lines (HEL and KG-1) were much less sensitive to AZD1152-hQPA than MOLM-13 and MEGAL cells were. MLN8054 markedly increased p-histone H3 except in MOLM-13 cells where the magnitude of SAC activation was notably lower. We observed a significantly lower level of aurora-A protein accumulation after nocodazole treatment in MOLM-13 cells than in KG-1, HEL, and MEGAL cells, suggesting the lower level of p-histone H3 accumulation after MLN8054 treatment may be due to a weakened SAC response in MOLM-13 cells (Supplementary Fig. S2). At higher concentrations of MLN8054 (≥ 2 μmol/L), we observed SAC silencing in three of four cell lines suggesting the compound can act as a pan-AKI. To confirm the mechanism of resistance to AZD1152-hQPA, we determined that HEL and KG-1 cells overexpress P-gp, and showed that co-administration of P-gp/BCRP1 inhibitor GF120918 (30, 32) re-sensitized HEL cells to AZD1152-hQPA relative to AMG 900 (Fig. 1D and E).

Author Manuscript Author Manuscript Author Manuscript Author Manuscript

Collectively, these data show that AMG 900 is more uniformly potent across AML lines with some overlapping and distinct features relative to isoform-selective AKIs.

AMG 900 induces polyploidization and differentiation of lineage-committed malignant megakaryocytes.

During normal maturation, megakaryocyte precursor cells become polyploid through a process termed endomitosis, where repeated rounds of DNA replication lead to large cells that permanently exit the cell cycle with nuclei containing 16N to 64N DNA content. Polyploidy inducers can fuel terminal differentiation of AMKL cells, producing similar cellular effects to those that occur during megakaryocyte maturation (18). To investigate the effects of pan-AK inhibition as a potential driver of cell differentiation, CHRF-288–11 AMKL cells were treated with AMG 900 or MLN8237. As shown in Figure 2A and B, both AKIs induced similar megakaryocyte maturation features as evidenced by the cell size, nuclear/cytoplasmic morphologies, level of polyploidization, and co-expression of CD41/CD42. Previous studies with MLN8237 demonstrated that inhibition of aurora-A promoted these same hallmarks of megakaryocyte maturation in HEL and SET-2 AML cell lines as well as in mouse bone marrow cells harboring *Jak2*^{V617F} knock-in mutation (16, 17). With this in mind, we investigated whether pan-AK inhibition would affect differentiation of *Jak2*^{V617F}-expressing mouse bone marrow cell cultures. As shown in Figure 2C and D, treatment with AMG 900 significantly increased polyploidization and expression of CD41/CD42 in a subset of mouse cells, where the level of differentiation was less for MLN8237 and failed to reach statistical significance.

AMG 900 induces apoptosis independent of p53 post-mitotic G1 checkpoint activation.

To examine the effects of pan-AK inhibition on p53 signaling we treated *TP53*^{WT} (GDM-1, MOLM-13) and *TP53*^{MUT} (U937, HEL) AML lines with AMG 900 for 48 hours. As shown in Figure 3A, AMG 900 markedly increased cl-caspase-3 protein levels in GDM-1, MOLM-13, and U937 cells, whereas HEL cells largely evaded apoptosis. Total p53 protein levels increased after AMG 900 treatment in both *TP53*^{WT} lines, which coincided with an increase in p21 protein levels in GDM-1 cells, but not in MOLM-13 cells. Surprised by these findings, we evaluated the p53 and p21 induction profile over a wider concentration range of AMG 900 in MOLM-13 cells and found a low level of p21 protein induction only near the inflection point (1.2 nmol/L), whereas p53 and cl-caspase-3 protein levels, and polyploidy increased in a parallel manner (Supplementary Fig. S3). In contrast to the other three AML lines, GDM-1 cells treated with AMG 900 showed a prominent 4N DNA content peak, consistent with attenuation of polyploidization mediated by p21-induced growth arrest (Fig. 3B) (33).

AMG 900 can potentiate cell killing in combination with LDAC.

To determine the effectiveness of AMG 900 in combination with LDAC, we designed a dose-matrix (1 to 4 nmol/L by 31 to 125 nmol/L, respectively) using U937, HEL, GDM-1, and MOLM-13 cells. After 72 hours, we determined the fraction of cells positive for apoptosis using annexin-V FC assay (Fig. 3C and D). The level of cell killing induced by combined AMG 900 and Ara-C varied, MOLM-13 and HEL showed a net increase in apoptosis relative to that induced by AMG 900 alone, whereas the combination was less

Author Manuscript Author Manuscript Author Manuscript Author Manuscript

effective than AMG 900 alone against U937 and GDM-1 cells. Based on the positive drug interaction on MOLM-13 cells, we next examined the cell cycle effects of combining AMG 900 and Ara-C. As shown in Figure 3E and F, we observed an increase in subG$_1$ and cl-caspase-3 gated populations (represented as total death) with a dose-dependent attenuation of polyploidization, suggesting the agents can act together to induce an effect not observed with either agent alone (neomorphic effect). Median dose-effect analysis using the Chou-Talalay method (34) showed that MOLM-13 cells treated with AMG 900 plus Ara-C combination in a cell growth assay had additive to weak synergy (combination index score of 1 to 0.7, respectively) (Supplementary Fig. S4).

Inhibition of aurora kinase activity in MOLM-13 cells by AMG 900 leads to accumulation of centrosomes, induction of the intrinsic apoptotic pathway, and cleavage of Bcl-2.

To understand the phenotypes and signaling events triggered by AMG 900, we selected MOLM-13 cells as a representative AML line for further studies. As shown in Figure 4A, DMSO-treated mitotic cells exhibited strong p-histone H3 immunoreactivity with condensed sister chromatids, and two centrosome centers. In contrast, AMG 900-treated mitotic cells showed a significant decrease in p-histone H3 associated with an accumulation of centrosomes and DNA content. Interestingly, a low-level of p-histone H3 signal was detectable in a subset of AMG 900 treated mitotic cells that had supernumerary centrosomes (eight pericentrin spots) and higher ploidy content (Fig. 4A, lower panel). One explanation for the residual p-histone H3 staining may be amplification of aurora-B gene dosage resulting from polyploidization. We next examined the effects of AMG 900 on intrinsic apoptotic pathway proteins (35) and compared the effects to an MDM2 inhibitor (nutlin-3a) (36). As shown in Figure 4B, AMG 900 increased total p53 and cl-caspase-3 protein levels with negligible changes in MDM2, p21, full-length Bcl-2, Mcl-1, Bcl-xL, and Bax protein levels. Notably, we detected a 23-kDa Bcl-2 protein product that mirrored the induction profile of cl-caspase-3 protein. Bcl-2 can convert from a full-length pro-survival protein to a lower molecular weight (LMW) form that is pro-apoptotic (37). The antibody used in our studies recognizes Bcl-2 peptide 41 to 54 a.a., that is downstream from two caspase cleavage sites (Asp-31, Asp-34); cleavage at these sites generates ~23-kDa protein product. Addition of caspase inhibitors (Z-VAD-fmk, Z-DEVD-fmk) attenuated the anti-proliferative effects of AMG 900 by ~2.5-fold relative to AKI treatment alone, and partially blocked apoptosis and Bcl-2 protein cleavage (Fig. 4C and D, Supplementary Fig. S5A and B). To examine the effects of AMG 900 on mitochondrial membrane (MM) integrity, we performed JC-1 coupled annexin-V analysis (Supplementary Fig. S6). In healthy mitochondria, JC-1 dye forms aggregates with orange-red fluorescence emission, during apoptosis, depolarization of the MM results in monomeric JC-1 with a green fluorescence emission profile (38). Treatment with AMG 900 increased the annexin-V population by 7-fold and decreased annexin-V positive JC-1 red fluorescence intensity by 5-fold, in agreement with cells undergoing apoptosis with de-energized MMs (Fig. 4E). Together, our results show that inhibition of aurora-B activity by AMG 900 in MOLM-13 cells leads to an increase in polyploidy and centrosome number, activation of p53 pathway without p21 induction, and increase in cell lethality mediated in part by the intrinsic apoptotic pathway.

Author Manuscript Author Manuscript Author Manuscript Author Manuscript

AMG 900 blocks proliferation of primary HBMNCs without inducing polyploidization.

In clinical studies, the most frequently observed adverse event with AKIs has been on-target myelotoxicity, particularly neutropenia (13–15, 29). To test the activity of AMG 900 on bone marrow suppression *in vitro*, we evaluated cultured HBMNCs that express granulocyte markers $CD15^+/CD11b^-$ (early myelocytes) and $CD15^+/CD11b^+$ (myelocytes to segmented granulocytes) (Supplementary Fig. S7A). We treated HBMNC cultures with AMG 900 or AZD1152-hQPA for 48 hours and observed an increase in cell death ($subG_1$) and a dose-dependent decrease in proliferation (BrdUrd uptake) with EC_{50} values similar to their potencies against AML cells (Supplementary Fig. S7B). To understand the potential recovery profile of normal cells after AKI washout, we shortened the duration of treatment to 24 hours and used anti-mitotic docetaxel as a cytotoxic comparator. In contrast to docetaxel, HBMNCs treated with AZD1152-hQPA or AMG 900 showed and improved recovery proliferation profile by 48 hours after compound washout, where AKIs were comparable to DMSO-treated cells (Supplementary Fig. S7C and S7D). No substantial accumulation of > 4N DNA content bone marrow cells was observed after treatment with AMG 900, suggesting pre- and/or post-mitotic mechanism (s) exist that prevent bulk polyploidization.

AMG 900 reduces tumor burden and inhibits [^{18}F]FLT uptake in the skeleton of mice bearing MOLM-13-Luc xenografts.

To examine the anti-proliferative effects of AMG 900 *in vivo*, we used a systemic AML model that closely mimics disease dissemination into the skeleton tissues of mice bearing MOLM-13 cells expressing luciferase (31). In addition, we utilized [^{18}F]FLT-PET/CT imaging as a noninvasive method of monitoring cell proliferation and drug response (39).

Nine days post-tumor implantation, mice were orally administered vehicle or AMG 900 using two dosing schedules (consecutive daily dosing for four days at 22 mg/kg or seven days at 12.6 mg/kg). Mice were imaged for luciferase activity and [^{18}F]FLT uptake before initiating treatment (baseline) and at multiple time points after the cessation of AMG 900 treatment as outlined in the study scheme in Figure 5A. As measured by whole body bioluminescence, mice treated with AMG 900 using either dose schedule showed significant anti-tumor activity across study time points relative to vehicle-treated group [tumor growth inhibition 86–90% and 94%, $P < .0001$ (days 6 and 9); 95%, $P < 0.02$ (day 12)] (Fig. 5B). Because of the aggressive nature of the MOLM-13 systemic model, animals with either hind-limb paralysis or significant body weight loss were euthanized. On average, mice maintained ≥ 90% of their initial body weight in all treatment groups, one animal from each treatment group died on study by day 19 post-tumor implantation (Supplementary Fig. S8). We removed the vehicle-treated group from study on day 19 and the AMG 900-treated groups on day 23. At the end of the study, we assessed mouse femurs for tumor burden by FC, using a DNA content fitting algorithm to quantify the ratio of mouse diploid cells to human aneuploid AML cells (Fig. 5C and D). Relative to vehicle-treated group, AMG 900 significantly reduced the MOLM-13 cell fraction in the marrow ($P \leq 0.0002$) (Fig. 5D), with 7-day schedule reducing tumor burden to a greater degree than the 4-day schedule ($P = 0.0152$).

Author Manuscript Author Manuscript Author Manuscript Author Manuscript

The combined approach of PET/CT offers the capability of high-resolution 3D imaging of skeletal tissue to measure and report [^{18}F]FLT signal specifically in bone as the percentage injected dose per gram of tissue (%ID/g). Mice were administered FLT radiotracer at baseline (one day before treatment) and on days 5, 8, 11, and 14 after the start of treatment (Fig. 5E and F). Administration of AMG 900 on 4-day and 7-day schedules significantly inhibited skeletal [^{18}F]FLT uptake measured on day 5 [22 mg/kg AMG 900 = 2.2 %ID/g ± 0.08; vehicle = 3.7 %ID/g ±0.23 ($P < 0.0001$)] and day 8 [12.6 mg/kg AMG 900 = 2.8 %ID/g ± 0.4; vehicle = 5.2 %ID/g ± 0.2 ($P < 0.0001$)], respectively. Interestingly, both AMG 900 schedules resulted in a [^{18}F]FLT flare event measured four days after treatment cessation (Fig. 5E, noted by the arrowheads). Skeletal [^{18}F]FLT signal decreased within three days after the initial flare event, suggesting the flare may have resulted from a transient pulse of proliferation associated with bone marrow recovery (40) or alternatively, may have resulted from a drug induced cell-cycle synchronization of remaining viable cancer cells.

Discussion

Despite recent advances in our understanding of AML molecular heterogeneity and pathogenesis (2), new-targeted treatment strategies have largely failed at improving overall survival over standard chemotherapy. In this report, AMG 900 distinguished itself as the most potent anti-leukemic agent across a panel of diverse AML cell lines compared against two AK isoform-selective inhibitors and two classic AML drugs. We established the primary effects of AMG 900 on AML cells resulted in suppression of p-histone H3, polyploidization and/or apoptosis with cellular effects mirroring that of AZD1152-hQPA, indicating inhibition of aurora-B as the dominant driver of anti-leukemic activity. Suppression of p-histone H3 immunoreactivity in AML or normal proliferating cells by AMG 900 may serve as a robust pharmacodynamic marker for monitoring aurora-B inhibition *in vivo* (41), whereas accurately measuring aurora-A inhibition *in vivo* remains a challenge for the field (42). Our cell line data supports that MLN8054 has a more complex concentration-dependent mode-of-action, either by activating SAC through selective inhibition of aurora-A, or by SAC silencing through dual AK inhibition at higher micromolar concentrations. Based on our current study, we cannot definitively conclude that dual AK inhibition is more efficient at killing AML cells than isoform-selective AK inhibition. However, in contrast to isoform-specific AKIs, dual AK inhibition by AMG 900 reduces the likelihood of resistance driven by target-modifying mutations, as both mitotic genes are essential for cell division (25). Multiple other factors can contribute to drug resistance including elevated expression of P-gp, which in elderly AML patients is strongly associated with negative outcomes (21, 43). Unlike the case with AZD1152-hQPA, cell surface expression of P-gp on AML cells did not confer resistance to AMG 900. Clinically, selection of AML patients based on P-gp expression level is one biomarker approach to assess the utility of AMG 900 at combating drug-efflux mediated resistance, particularly in a relapse setting. Conversely, AMG 900 could negatively impact cycling immature hematopoietic progenitor cells expressing P-gp and BCRP1.

A subset of bone marrow proliferative disorders such as AMKL and PMF are characterized by defects in megakaryocyte differentiation. AMG 900-treatment of AMKL and *Jak2*^{V617F} mutant cells induced parallel increases in DNA ploidy, cytoplasmic volume, and expression

Author Manuscript Author Manuscript Author Manuscript Author Manuscript

of CD41/CD42, all three phenotypes associated with megakaryocyte maturation. Admittedly, this same assessment should be expanded to include AZD1152-hQPA to determine whether selective aurora-B and dual AK inhibition induce similar hallmarks of megakaryocyte maturation (16). Induction of differentiation with all-*trans* retinoic acid is a successful strategy for treating acute promeylocytic leukemia (44), whether this approach can be efficacious with induction of polyploidization (18) is actively under investigation with alisertib in AMKL and PMF patients.

In the next phase of our *in vitro* studies, we determined that AMG 900 combined with LDAC either enhanced (HEL, MOLM-13) or attenuated cell killing (GDM-1, U937). The observation that $TP53^{WT}$ GDM-1 cells showed a strong cell arrest response after AMG 900 treatment suggests p21 protein induction promotes an antagonistic interaction with Ara-C in terms of lethality. Evaluating AK inhibition in combination with Ara-C in a larger panel of AML lines and primary AMLs representing diverse FAB subtypes and genotypes is an appropriate next step to better define the response differences observed in our study and to elucidate the molecular underpinnings driving enhanced cell killing. In a phase-1 AML study with AMG 900, baseline expression levels of select mitotic genes (*AURKA*, *AURKB*, *BIRC5*, *CCNB1*, *CDC2*, *TTK*) were evaluated in 24 patients as exploratory biomarkers. Of note, three CRi responders to AMG 900 all showed elevated expression of mitotic genes at baseline (29). While these results are interesting, additional studies are needed due to the small sample size. One unanticipated finding from our *in vitro* studies was the detection of a LMW-form of Bcl-2 protein after AMG 900 treatment in MOLM-13 cells. Cleavage of Bcl-2 is believed to inactivate its pro-survival function, consistent with our observation that peptide caspase inhibitors attenuated the apoptotic response of AMG 900 noted by the concomitant drop in active-caspase-3 and LMW-form of Bcl-2 protein levels. We detected no changes in the ratio of Bcl-2 to Bax protein expression with AMG 900, which was previously reported to be positive predictor of pro-apoptotic response in AML lines treated with pan-AKI VX-680 (35). In this report, we did not directly address the cell fate of cycling polyploid AML cells harboring extra centrosomes after AKI withdrawal. Given that SAC silencing by AMG 900 leads to exit from mitosis without division, the likelihood of a mitotic catastrophe event with AKI present is low. However, upon SAC restoration after AMG 900 wash out, polyploid AML cells that transition through mitosis are expected to trigger lethal multipolar cell division and/or cellular senescence in the next interphase.

On-mechanism toxicity to normal proliferating tissues has hindered clinical development of small molecule inhibitors targeting mitotic kinases and kinesins (45). Consistent with this anti-mitotic class effect, AMG 900 induced cytotoxicity on HBMNCs in culture; however, we did observe an improved time-to-recovery profile after AMG 900 washout relative to classic anti-mitotic agent docetaxel. Several factors have the potential to influence efficacy/toxicity profile such as individual AKI drug-like properties, dose scheduling, route of administration, and formulation. One recent approach aimed at improving the effectiveness of AZD1152-hQPA used a nanoparticle formulation and an alternative dose schedule to successfully demonstrate durable regressions in AML xenograft models with lower toxicity (46); this same strategy is now in clinical testing with AZD1152-hQPA in AML and myelodysplastic syndrome patients (NCT03217838).

Author Manuscript Author Manuscript Author Manuscript Author Manuscript

In line with our *in vitro* results, AMG 900 demonstrates robust anti-leukemia activity in an aggressive MOLM-13 systemic xenograft model, in which tumor burden was determined by whole body bioluminescence and AML cell dissemination in skeletal tissue. A single cycle of AMG 900 treatment using two clinically relevant schedules (4-day and 7-day) (29) resulted in significant tumor growth inhibition (>85% TGI) by BLI. We also observed a reduction in tumor burden in mouse femurs, where the 7-day schedule appeared to be more effective at clearing AML cells from the bone. Additional studies will be required using multiple cycles of AMG 900 treatment in a less aggressive AML xenograft model to assess anti-leukemia durability. In order to correlate the anti-tumor effects of AMG 900 more directly, we assessed active DNA replication (S-phase) fraction using radiotracer [^{18}F]FLT-PET in skeletal tissue. Factors that influence [^{18}F]FLT-PET signal output after AKI treatment may include differences in proliferation rates between bone marrow and AML cells, thymidine kinase 1 expression, and the level of polyploidization (40, 47). With those stated factors, we clearly demonstrated AMG 900 reduced skeletal [^{18}F]FLT signal during the treatment phase followed by an [^{18}F]FLT flare event after treatment cessation, which may have resulted from bone marrow recovery and/or AML cells re-entering S-phase. Based on these data, [^{18}F]FLT-PET imaging could be used to further optimize AMG 900 dose scheduling and explore multidrug combinations. Importantly from a therapeutic perspective, Ara-C is a cell-cycle phase specific nucleoside that kills cells in S-phase (48), therefore one could hypothesize that induction of an AMG 900 [^{18}F]FLT flare event followed by LDAC may prime leukemia cells for maximal killing and thereby improve durability of response.

In summary, we provide evidence that AMG 900 has potent anti-leukemia activity on a panel of AML lines and that it can cooperatively promote enhanced cell killing in combination with LDAC. Cellular effects of AMG 900 were similar to AZD1152-hQPA, with differences in activity due to drug-efflux and kinase specificity. We discovered AMG 900 triggers maturation of AMKL and *Jak2*^{V617F} cells, suggesting it can act as a differentiation inducer. Our work provides an initial framework in which AMG 900 can serve as a best-in-class pan-AKI for further exploration of the effects of AKIs on the interconnected p53/apoptotic/mitotic signaling networks in AML. Lastly, we highlight the *in vivo* activity of AMG 900 in a systemic AML model and the utility of [^{18}F]FLT-PET/CT imaging for monitoring drug action.

Supplementary Material

Refer to Web version on PubMed Central for supplementary material.

Acknowledgments

The authors thank individuals on AMG 900 project and specifically Stephanie Geuns-Meyer, Kathleen Keegan, Gregory Friberg, Erick Gamelin, Richard Kendall, Peter Pieslor, and Florian Vogl. We thank Ann Mullally at Brigham and Women's Hospital/Harvard Medical School for providing the *Jak2*^{V617F} mice. This work was supported in part by a grant from the NIH (HL112792) to JDC. We would also like to acknowledge the team from Molecular Imaging Inc. and inviCRO Inc. for conducting the *in vivo* imaging studies.

Author Manuscript Author Manuscript Author Manuscript Author Manuscript

References

1. Siegel RL, Miller KD, Jemal A. Cancer statistics, 2015. CA: A Cancer J for Clinicians. 2015;65:5–29.
2. Dohner H, Weisdorf DJ, Bloomfield CD. Acute Myeloid Leukemia. N Engl. J Med 2015;373:1137–51.
3. Stone RM, Mandrekar SJ, Sanford BL, Laumann K, Geyer S, Bloomfield CD, et al. Midostaurin plus chemotherapy for acute myeloid leukemia with a FLT3 mutation. N Engl. J Med. 2017;377:454–64. [PubMed: 28644114]
4. Laubach J, Rao AV. Current and emerging strategies for the management of acute myeloid leukemia in the elderly. The Oncologist 2008;13:1097–1108. [PubMed: 18922830]
5. Lens SM, Voest EE, Medema RH. Shared and separate functions of polo-like kinases and aurora kinases in cancer. Nat Rev Cancer. 2010;10:825–41. [PubMed: 21102634]
6. Gautschi O, Heighway J, Mack PC, Purnell PR, Lara PN, Gardara DR et al. Aurora kinases as anticancer drug targets. Clin Cancer Res 2008;14:1639–48. [PubMed: 18347165]
7. Ikezoe T, Yang J, Nishioka C, Tasaka T, Taniguchi A, Kuwayama Y et al. A novel treatment strategy targeting Aurora kinases in acute myelogenous leukemia. Mol Cancer Ther 2007;6:1851–57. [PubMed: 17541033]
8. Goldenson B, Crispino JD. The aurora kinases in cell cycle and leukemia. Oncogene 2015;34:537–45. [PubMed: 24632603]
9. Manfredi MG, Ecsedy JA, Meetze KA, Balani SK, Burenkova O, Chen W, et al. Antitumor activity of MLN8054, an orally active small-molecule inhibitor of Aurora A kinase. PNAS 2007;104:4106–11. [PubMed: 17360485]
10. Sells TB, Chau R, Ecsedy JA, Gershman RE, Hoar K, Huck J et al. MLN8054 and Alisertib (MLN8237): discovery of selective oral Aurora A inhibitors. ACS Med Chem Letters. 2015;6:630–34.
11. Oke A, Pearce D, Wilkinson RW, Crafter C, Odedra R, Cavenagh J et al. AZD1152 rapidly and negatively affects the growth and survival of human acute myeloid leukemia cells in vitro and in vivo. Cancer Res 2009;15;69:4150–58.
12. Grundy M, Seedhouse C, Shang S, Richardson J, Russell N, Pallis M. The FLT3 internal tandem duplication mutation is a secondary target of the aurora B kinase inhibitor AZD1152-HQPA in acute myelogenous leukemia cells. Mol Cancer Ther 2010;9:661–72. [PubMed: 20159992]
13. Goldberg SL, Fenaux P, Craig MD, Gyan E, Lister J, Kassis J et al. . An exploratory phase 2 study of investigational Aurora A kinase inhibitor alisertib (MLN8237) in acute myelogenous leukemia and myelodysplastic syndromes. Leuk Res Reports 2014;3:58–61.
14. Löwenberg B, Muus P, Ossenkoppele G, Rousselot P, Cahn JY, Ifrah N et al. Phase 1/2 study to assess the safety, efficacy, and pharmacokinetics of barasertib (AZD1152) in patients with advanced acute myeloid leukemia. Blood 2011;118:6030–36. [PubMed: 21976672]
15. Kantarjian HM, Martinelli G, Jabbour EJ, Quintás-Cardama A, Ando K, Bay JO et al. . Stage I of a phase 2 study assessing the efficacy, safety, and tolerability of barasertib (AZD1152) versus low-dose cytosine arabinoside in elderly patients with acute myeloid leukemia. Cancer. 2013;119:2611–9. [PubMed: 23605952]
16. Wen QJ, Goldenson B, Silver SJ, Schenone M, Dancik V, Huang Z et al. Identification of regulators of polyploidization presents therapeutic targets for treatment of AMKL. Cell. 2012;150:575–89. [PubMed: 22863010]
17. Wen QJ, Yang Q, Goldenson B, Malinge S, Lasho T, Schneider RK, et al. Targeting megakaryocytic-induced fibrosis in myeloproliferative neoplasms by AURKA inhibition. Nat Med 2015;21:1473–80. [PubMed: 26569382]
18. Krause DS, Crispino JD. Molecular pathways: induction of polyploidy as a novel differentiation therapy for leukemia. Clin Cancer Res 2013;19 :6084–88. [PubMed: 23963861]
19. Wiseman DH, Greystoke BF, Somervaille TCP. The variety of leukemia stem cells in myeloid malignancy. Oncogene 2014;33: 3091–98. [PubMed: 23831573]

Author Manuscript Author Manuscript Author Manuscript Author Manuscript

20. Stiehl T, Baran N, Ho AD, Marciniak-Czochra A. Cell division patterns in acute myeloid leukemia stem-like cells determine clinical course: a model to predict patient survival. Cancer Res 2015;75:940–49. [PubMed: 25614516]
21. Xia CQ, Smith PG. Drug efflux transporters and multidrug resistance in acute leukemia: therapeutic impact and novel approaches to mediation. Mol Pharm 2012;82:1008–21.
22. Grundy M, Seedhouse C, Russell NH, Pallis M. P-glycoprotein and breast cancer resistance protein in acute myeloid leukaemia cells treated with the aurora-B kinase inhibitor barasertib-hQPA. BMC Cancer. 2011;11 :254.1–13. [PubMed: 21679421]
23. Girdler F, Sessa F, Patercoli S, Villa F, Musacchio A, Taylor S. Molecular basis of drug resistance in aurora kinases. Chem & Biol 2008:23;15:552–62.
24. Payton M, Bush TL, Chung G, Ziegler B, Eden P, McElroy P, et al. Preclinical evaluation of AMG 900, a novel potent and highly selective pan-aurora kinase inhibitor with activity in taxane-resistant tumor cell lines. Cancer Res 2010;70:9846–54. [PubMed: 20935223]
25. Geuns-Meyer S, Cee VJ, Deak HL, Du B, Hodous BL, Nguyen HN et al. Discovery of N-(4-(3-(2-aminopyrimidin-4-yl) pyridin-2-yloxy) phenyl)-4-(4-methylthiophen-2-yl) phthalazin-1-amine (AMG 900), a highly selective, orally bioavailable inhibitor of aurora kinases with activity against multidrug-resistant cancer cell lines. J Med Chem 2015;58:5189–207. [PubMed: 25970324]
26. Bush TL, Payton M, Heller S, Chung G, Hanestad K, Rottman JB et al. AMG 900, a small-molecule inhibitor of aurora kinases, potentiates the activity of microtubule-targeting agents in human metastatic breast cancer models. Mol Cancer Ther 2013;12:2356–66. [PubMed: 23990115]
27. Kalous O, Conklin D, Desai AJ, Dering J, Goldstein J, Ginther C et al. AMG 900, pan-Aurora kinase inhibitor, preferentially inhibits the proliferation of breast cancer cell lines with dysfunctional p53. Breast Cancer Res and Treatment. 2013;141:397–408.
28. Paller CJ, Wissing MD, Mendonca J, Sharma A, Kim E, Kim HS et al. Combining the pan-aurora kinase inhibitor AMG 900 with histone deacetylase inhibitors enhances antitumor activity in prostate cancer. Cancer Med 2014;3:1322–35. [PubMed: 24989836]
29. Kantarjian HM, Schuster MW, Jain N, Advani A, Jabbour E, Gamelin E et al. A phase 1 study of AMG 900, an orally administered pan-aurora kinase inhibitor, in adult patients with acute myeloid leukemia. Am J Hematol 2017;92:660–67. [PubMed: 28370201]
30. Hyafil F, Vergely C, Du Vignaud P, Grand-Perret T. In vitro and in vivo reversal of multidrug resistance by GF120918, an acridonecarboxamide derivative. Cancer Research. 1993;53:4595–602. [PubMed: 8402633]
31. Keegan K, Li C, Li Z, Ma J, Ragains M, Coberly S et al. Preclinical evaluation of AMG 925, a FLT3/CDK4 dual kinase inhibitor for treating acute myeloid leukemia. Mol Cancer Ther 2014;13:880–9. [PubMed: 24526162]
32. Szakács G, Paterson JK, Ludwig JA, Booth-Genthe C, Gottesman MM. Targeting multidrug resistance in cancer. Nat Rev Drug Disc 2006;5:219–34.
33. Ikezoe T, Yang J, Nishioka C, Yokoyama A. p53 is critical for the Aurora B kinase inhibitor-mediated apoptosis in acute myelogenous leukemia cells. Int J Hematol 2010;91:69–77. [PubMed: 20013323]
34. Chou TC. Theoretical basis, experimental design, and computerized simulation of synergism and antagonism in drug combination studies. Pharmacological Rev 2006;58:621–81.
35. Huang XF, Luo SK, Xu J, Li J, Xu DR, Wang LH, Yan M, Wang XR, Wan XB, Zheng FM, Zeng YX. Aurora kinase inhibitory VX-680 increases Bax/Bcl-2 ratio and induces apoptosis in Aurora-A-high acute myeloid leukemia. Blood 2008;111:2854–65. [PubMed: 18160664]
36. Kojima K, Konopleva M, Samudio IJ, Shikami M, Cabreira-Hansen M, McQueen T et al. MDM2 antagonists induce p53-dependent apoptosis in AML: implications for leukemia therapy. Blood 2005;106:3150–9. [PubMed: 16014563]
37. Fadeel B, Hassan Z, Hellström-Lindberg E, Henter JI, Orrenius S, Zhivotovsky B. Cleavage of Bcl-2 is an early event in chemotherapy-induced apoptosis of human myeloid leukemia cells. Leukemia 1999;13:719–28. [PubMed: 10374876]
38. Salvioli S, Ardizzoni A, Franceschi C, Cossarizza A. JC 1, but not DiOC6 (3) or rhodamine 123, is a reliable fluorescent probe to assess ΔΨ changes in intact cells: implications for studies on mitochondrial functionality during apoptosis. FEBS letters. 1997;411:77–82. [PubMed: 9247146]

Author Manuscript Author Manuscript Author Manuscript Author Manuscript

39. Vanderhoek M, Juckett MB, Perlman SB, Nickles RJ, Jeraj R. Early assessment of treatment response in patients with AML using [18 F] FLT PET imaging. Leukemia Res 2011;35:310–6. [PubMed: 20832860]
40. Schelhaas S, Held A, B€aumer N, Viel T, Hermann S, M€uller-Tidow C, Jacobs AH. Preclinical evidence that 3'-Deoxy-3'-[18F]Fluorothymidine PET can visualize recovery of hematopoiesis after gemcitabine chemotherapy. Cancer Res 2016:76;7089–95. [PubMed: 27923827]
41. Juan G, Bush TL, Ma C, Manoukian R, Chung G, Hawkins JM, et al. AMG 900, a potent inhibitor of aurora kinases causes pharmacodynamic changes in p-Histone H3 immunoreactivity in human tumor xenografts and proliferating mouse tissues. Journal of Translational Medicine. 2014;12:307. [PubMed: 25367255]
42. Shagisultanova E, Dunbrack RL, Golemis EA. Issues in interpreting the in vivo activity of Aurora-A inhibitors. Expert Opin Ther Targets 2015:19: 187–200. [PubMed: 25384454]
43. Leith CP, Kopecky KJ, Godwin J, McConnell T, Slovak ML, Chen IM et al. Acute myeloid leukemia in the elderly: assessment of multidrug resistance (MDR1) and cytogenetics distinguishes biologic subgroups with remarkably distinct responses to standard chemotherapy. A Southwest Oncology Group study. Blood 1997;89:3323–9. [PubMed: 9129038]
44. Tallman MS, Andersen JW, Schiffer CA, Appelbaum FR, Feusner JH, Ogden A, et al. All-trans-retinoic acid in acute promyelocytic leukemia. N Engl J Med 1997;337:1021–28. [PubMed: 9321529]
45. Mitchison TJ. The proliferation rate paradox in antimitotic chemotherapy. Mol Biol Cell 2012;23:1–6. [PubMed: 22210845]
46. Floc'h N, Ashton S, Taylor P, Trueman D, Harris E, Odedra R, et al. Optimizing Therapeutic Effect of Aurora B Inhibition in Acute Myeloid Leukemia with AZD2811 Nanoparticles. Mol Cancer Ther 2017;16:1031–40. [PubMed: 28292940]
47. Been LB, Suurmeijer AJ, Cobben DC, Jager PL, Hoekstra HJ, Elsinga PH. [18F] FLT-PET in oncology: current status and opportunities. Eur J Nucl Med Mol Imaging 2004;31:1659–72. [PubMed: 15565331]
48. Sampath D, Rao VA, Plunkett W. Mechanisms of apoptosis induction by nucleoside analogs. Oncogene 2003;22:9063–74. [PubMed: 14663485]

Author Manuscript Author Manuscript Author Manuscript Author Manuscript

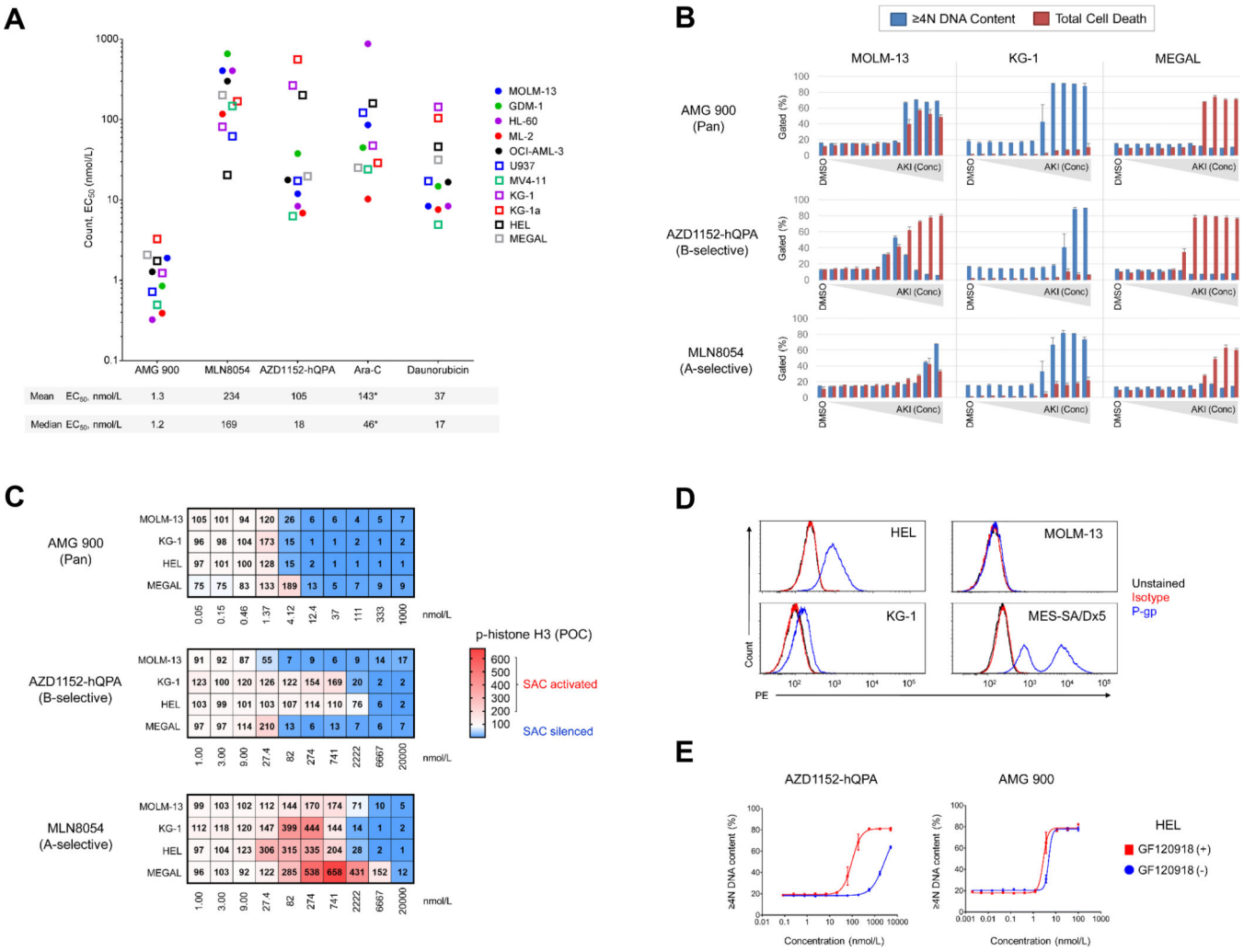

Figure 1.

AMG 900 exhibits potent anti-leukemia activity on AML cell lines with a distinct sensitivity profile relative to isoform-selective AKIs. **A** and **B,** AML cell lines were treated with DMSO or test agents at eleven concentrations [three-point dilution, high concentration AMG 900 (0.1 μmol/L), MLN8054 and AZD1152-hQPA (5 μmol/L), Ara-C and daunorubicin (20 μmol/L)] for 72 hours. Cell count and apoptosis/DNA content analysis. **A,** Cell count potency determined for individual AML lines (n = 11), with mean and median EC_{50} values noted below. *OCI-AML-3 data not included in graph for Ara-C (EC_{50} > 1 μmol/L). **B,** AKI dose-response profiles for MOLM-13, KG-1a, and HL-60 cells showing percentage of ≥ 4N DNA content and total cell death ($subG_1$ + cl-caspase-3) populations (mean ± SD). **C,** MOLM-13, KG-1, HEL, and MEGAL cells treated with AMG 900, MLN8054, and AZD1152-hQPA or DMSO for 48 hours. Heatmaps showing p-histone H3 positivity represented as a mean percentage of control (POC). SAC activation (p-histone H3 POC > 100, *white* to *red*) and SAC silencing (p-histone H3 POC < 100, *white* to *blue*). **D,** Histogram of MOLM-13, KG-1, HEL cells stained with P-gp (*blue*) and isotype (*red*) antibodies, and unstained control (*black*). MES-SA/Dx5 cells were included as P-gp control. **E,** DNA content analysis of HEL cells treated with AMG 900 or AZD1152-hQPA ± P-gp

inhibitor GF120918. Dose-response of AKI alone (*blue*) and in combination with P-gp inhibitor (*red*).

Author Manuscript Author Manuscript Author Manuscript Author Manuscript

Author Manuscript Author Manuscript Author Manuscript Author Manuscript

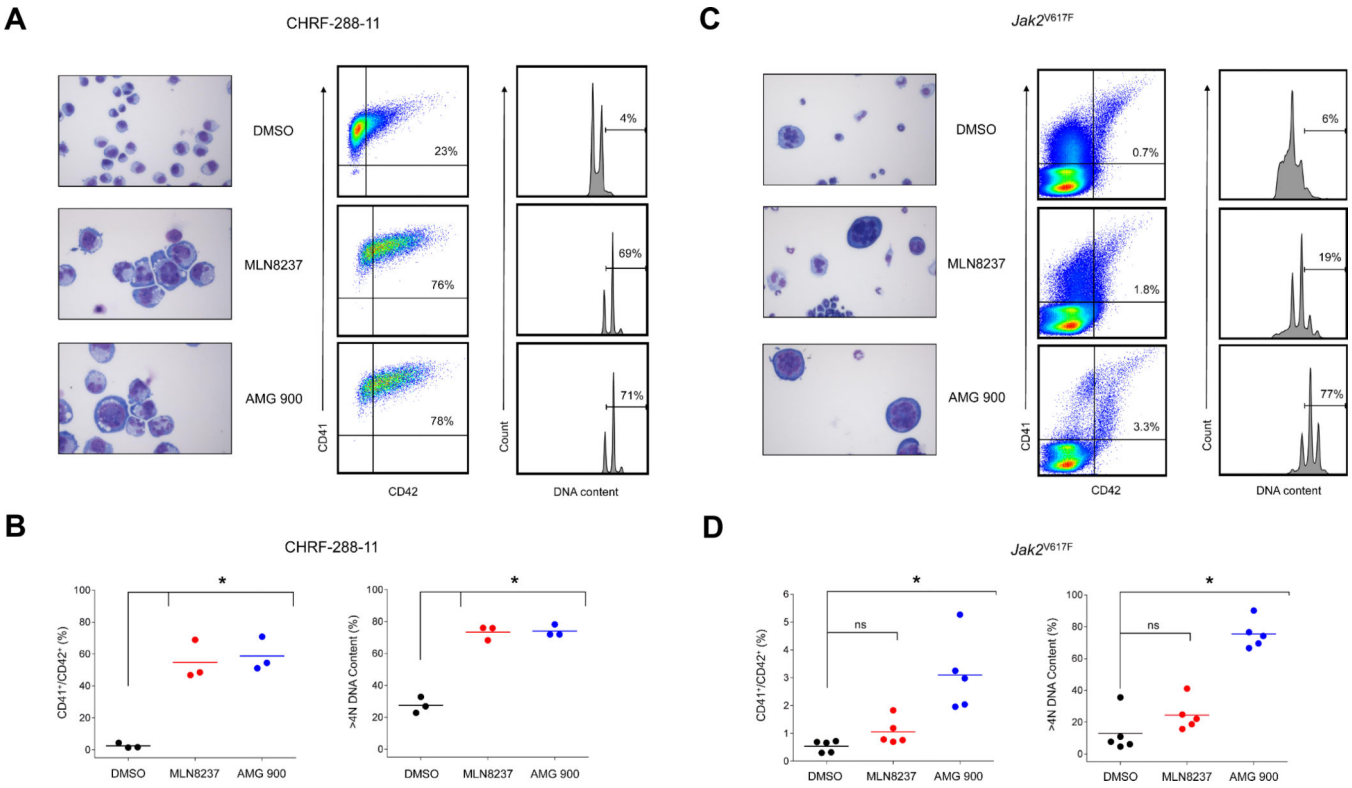

Figure 2.

AMG 900 induces polyploidization and the expression of megakaryocyte-lineage differentiation markers. CHRF-288–11 AMKL cells and *Jak2*^{V617F} knock-in mouse bone marrow cells were treated with MLN8237 and AMG 900 at 0.3 μmol/L or DMSO for 72 hours. **A** and **C,** Representative images of Wright-Giemsa stained cells (magnification x400), CD41/CD42 expression, and DNA content profiles. **B** and **D,** Percentage of CD41^{+}/CD42^{+} and > 4N DNA content gated CHRF-288–11 and *Jak2*^{V617F} gated populations (mean ± SD). CHRF-288–11 cells [MLN8237 and AMG 900 versus DMSO (CD41^{+}/CD42^{+} and DNA ploidy, $*P \leq 0.0009$)]. *Jak2*^{V617F} cells from five individual mice [MLN8237 versus DMSO (CD41^{+}/CD42^{+} $P = 0.1993$, DNA ploidy $P = 0.5334$, not significant (ns); AMG 900 versus DMSO (CD41^{+}/CD42^{+} and DNA ploidy $*P \leq 0.0007$)].

Author Manuscript Author Manuscript Author Manuscript Author Manuscript

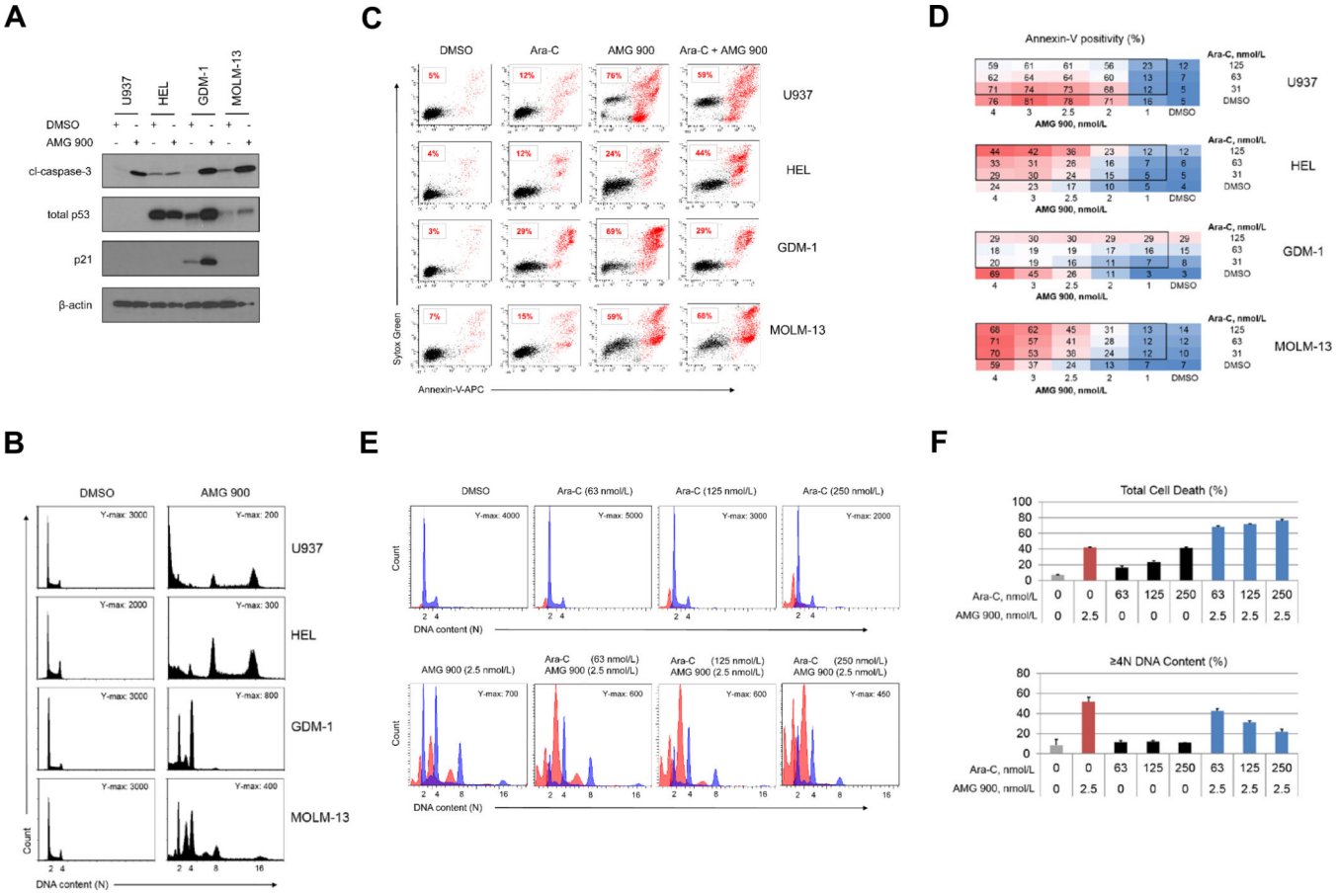

Figure 3.

AMG 900 can increase polyploidy, apoptosis, and p53 protein levels in AML cell lines, and can potentiate the activity of LDAC. **A** and **B,** U937 (*TP53*^{MUT}), HEL (*TP53*^{MUT}), GDM-1 (*TP53*^{WT}), and MOLM-13 (*TP53*^{WT}) cells were treated with AMG 900 at 33 nmol/L or DMSO for 48 hours. Western blot and cell-cycle analysis. **A,** Protein expression profiles of cl-caspase-3, total p53, p21, and β-actin. **B,** DNA content profiles with indicated Y-axis maximal (Y-max) count and ploidy (2N to 16N). **C** and **D,** AML cells treated with AMG 900, Ara-C, or DMSO, and in combination using 4 × 3 dose-matrix for 72 hours. Annexin-V apoptosis analysis. **C,** Representative scatter plots of annexin-V positivity percentages (*red*) for test agent alone and combined AMG 900 (4.0 nmol/L) and Ara-C (125 nmol/L). **D,** Percentage of annexin-V positivity across dose-matrix. **E** and **F,** MOLM-13 cells were treated with test agent alone at the indicated concentrations and in combination for 72 hours. Apoptosis and cell-cycle analysis. **E,** DNA content profiles with cl-caspase-3 positive population (*red*) with Y-max count and ploidy (2N to 16N). **F,** Percentage of total cell death (subG$_1$ + cl-capase-3) and ≥ 4N DNA content (mean ± SD).

Author Manuscript Author Manuscript Author Manuscript Author Manuscript

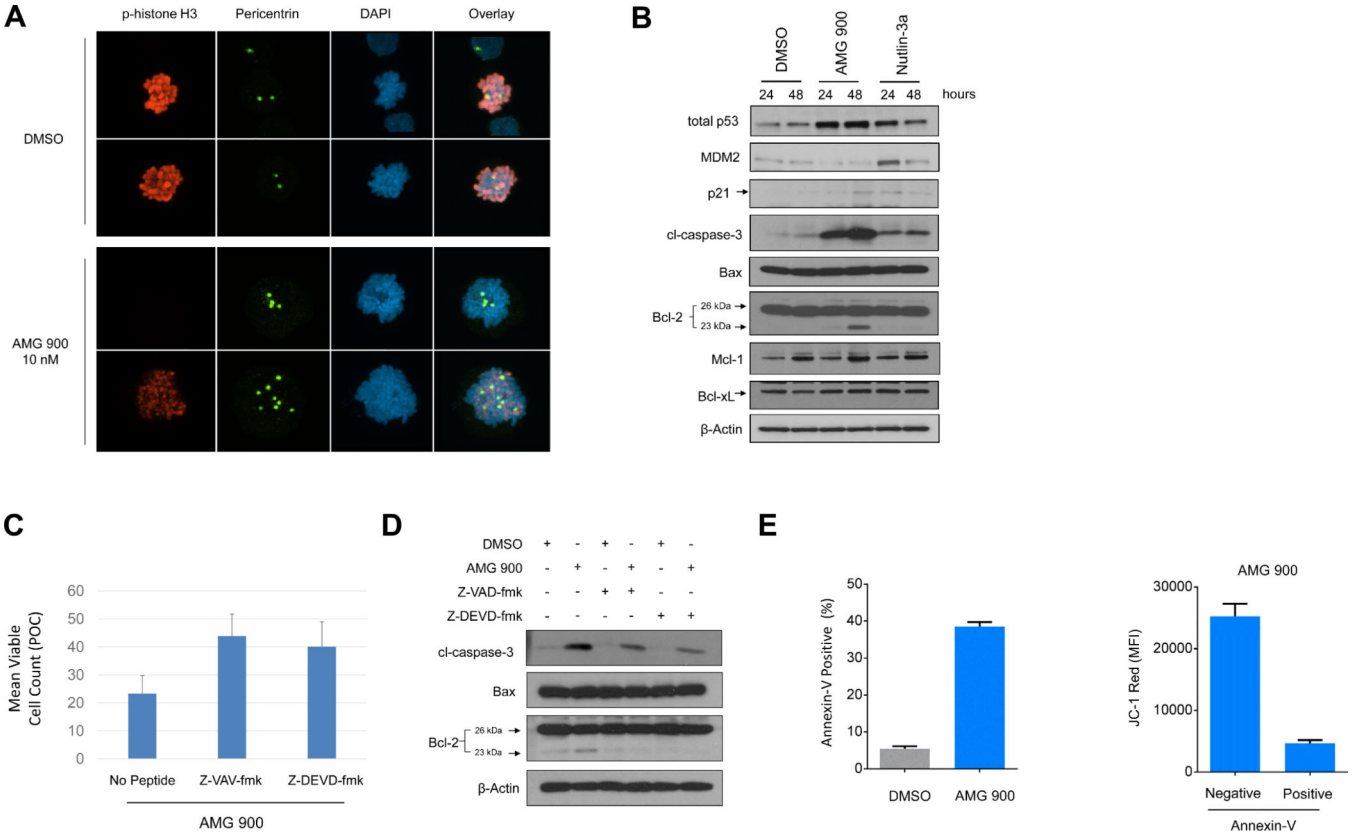

Figure 4.

Inhibition of aurora-B activity by AMG 900 leads to polyploidization associated with extra centrosomes, induction of apoptosis, and Bcl-2 cleavage in MOLM-13 cells. **A,** Cells were treated with AMG 900 at 10 nmol/L or DMSO for 48 hours. Representative confocal images of treated mitotic cells stained with p-histone H3 (*red*) and pericentrin (*green*) antibodies and DAPI (*blue*) (magnification x600). **B,** Cells treated with AMG 900 at 33 nmol/L, nutlin-3a at 2.5 μmol/L, or DMSO for 24 and 48 hours. Western blot analysis showing protein expression of total p53, MDM2, p21, cl-caspase-3, Bax, Bcl-2, Mcl-1, Bcl-xL, and β-actin. Arrows indicate specific target protein band. **C** and **D,** Cells pre-incubated ± caspase inhibitors (Z-VAV-fmk, Z-DEVD-fmk) at 10 μmol/L for 2 hours before treatment with AMG 900 at 33 nmol/L or DMSO for 48 hours. Cell count and Western blot analysis. **C,** Cell count represented as POC (mean ± SD). **D,** Protein expression profile of cl-caspase-3, Bax, Bcl-2, and β-actin. **E,** Cells treated with AMG 900 at 33 nmol/L or DMSO for 48 hours. Annexin-V/JC-1 analysis. Measurement of annexin-V positivity percentage (left graph, mean ± SD) and JC-1 dye red mean fluorescence intensity (MFI) for AMG 900 treated annexin-V negative and positive populations (right graph, mean ± SD).

Author Manuscript Author Manuscript Author Manuscript Author Manuscript

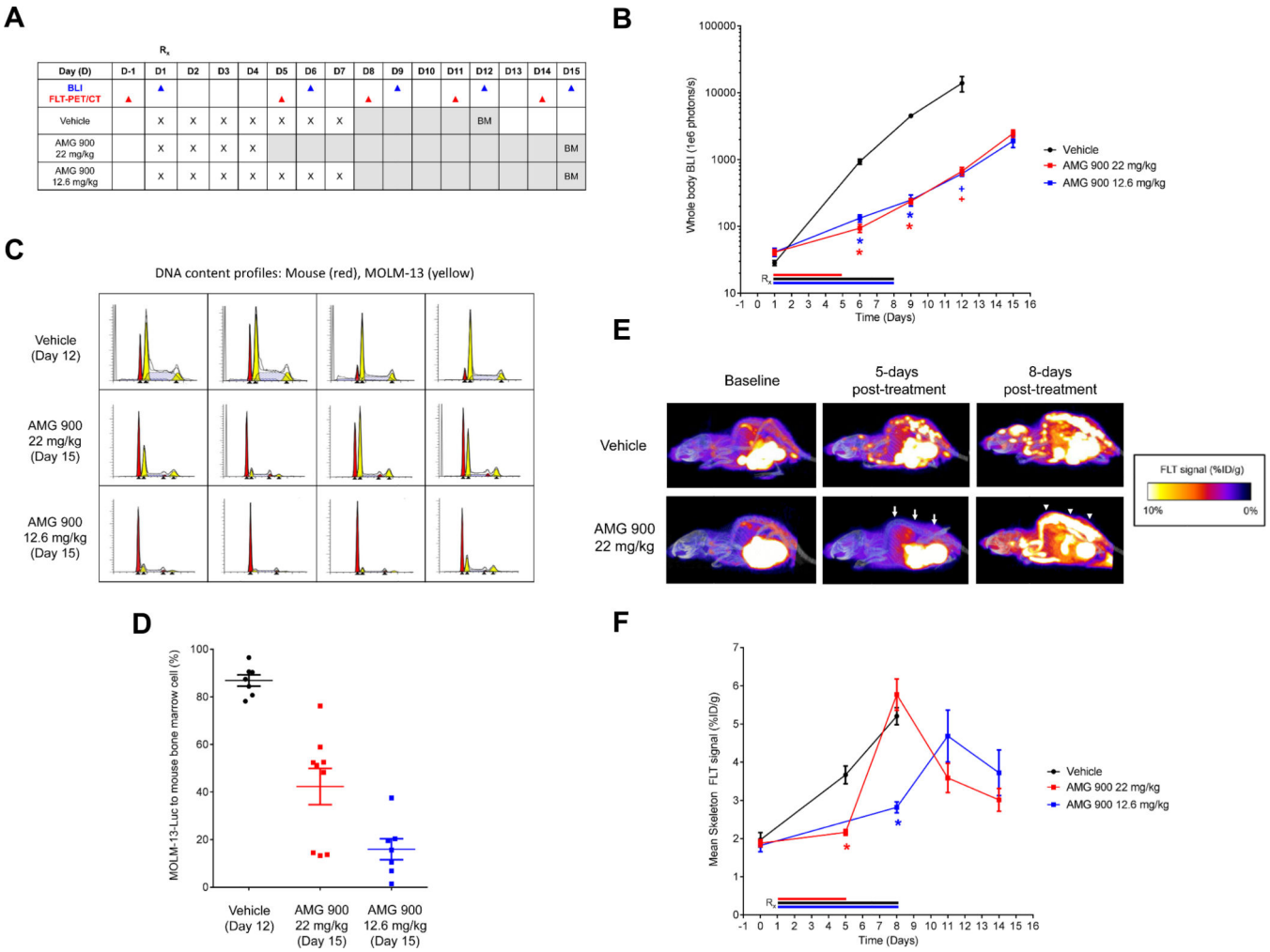

Figure 5.

Anti-leukemia activity of AMG 900 in a systemic MOLM-13 tumor xenograft model. Mice bearing established MOLM-13-Luc tumors were orally administered vehicle, AMG 900 at 12.6 mg/kg for 7 days or 22 mg/kg for 4 days (n = 10 per group). **A,** Outline of AMG 900 treatment and biomarker assessment schedule. Whole body BLI was recorded on days 1, 6, 9, 12, 15 (*blue*, ▲). [^{18}F]FLT-PET/CT measurements were determined the day before treatment (D-1, baseline), and on days 5, 8, 11, and 14 (*red*, ▲). Bone marrow (BM) aspirates were collected at study termination [vehicle (day 12) and AMG 900 (day 15)]. **B,** Tumor burden was determined by BLI (mean ± SE) for vehicle (*black*, ●, n = 9 on day 12), AMG 900 at 12.6 mg/kg (*blue*, ■, n = 9 on day 12), and AMG 900 at 22 mg/kg (*red*, ■, n = 9 on day 12) groups. Removed one animal from each group due to toxicity by day 12. Entire vehicle group was removed on day 12 due to morbidity. Statistical significance determined for AMG 900 groups versus vehicle on days 6, 9, and 12 (*$P < 0.0001$, $^{+}P < 0.02$). **C** and **D,** Tumor burden measured in femur BM aspirates by DNA content analysis. **C,** Representative fitted DNA content profiles from each treatment group, mouse BM (*red*) and MOLM-13-Luc (*yellow*) cell populations (detected G_1 and G_2 peaks, ▲). **D,** Percentage of tumor to BM cell population based on DNA content (mean ± SE). Statistical significance determined for

Author Manuscript Author Manuscript Author Manuscript Author Manuscript

AMG 900 22 mg/kg (n = 9) and 12.6 mg/kg (n = 7) groups versus vehicle (n = 7) ($P \leq$ 0.0002). **E** and **F,** [^{18}F]FLT-PET/CT imaging of skeleton tissue. [^{18}F]FLT signal was measured at baseline (1 day before treatment) and on days 5, 8, 11, and 14. **E,** Representative images of FLT signal at baseline, and day 5 and 8 post-treatment with AMG 900 at 22 mg/kg or vehicle for 4 days. [^{18}F]FLT signal suppression (*arrow*) and [^{18}F]FLT flare (*arrowhead*) indicated for AMG 900 treatment on day 5 and 8, respectively. **F,** Skeleton [^{18}F]FLT signal measured as percentage %ID/g (mean ± SE). Statistical significance determined for AMG 900 groups versus vehicle (*P < 0.0001, n = 9 to 10 per group).